Simulation results of transverse-optical confinement in airpost, regrown, and oxidized vertical-cavity surface-emitting laser structures

Peter Bienstman, Bart Demeulenaere,* Bart Dhoedt, and Roel Baets

Department of Information Technology, University of Gent, Sint-Pietersnieuwstraat 41, B-9000 Gent, Belgium

Based on a numerical optical model for calculating threshold material gain in vertical-cavity surface-emitting laser, we investigate the influence of transverse-optical confinement in airpost, regrown, and oxidized structures. In each of these cases, we demonstrate the trade-off that needs to be made between low threshold for the fundamental laser mode and good modal stability. © 1999 Optical Society of America
[S0740-3224(99)00411-7]
OCIS codes: 140.3430, 250.7260.

1. INTRODUCTION

In the design of today's high-performance vertical-cavity surface-emitting lasers (VCSEL's), it is of paramount importance to introduce some form of transverse-optical confinement for the laser beam. One can do this either by etching airpost pillars or by introducing an oxide aperture into the cavity. When it is carefully designed, the transverse waveguiding that is created in this way can counteract diffraction and improve modal stability. At the same time, these structures also provide current confinement. The importance of transverse confinement is illustrated by the high performance achieved by today's oxide-apertured VCSEL's, which includes low threshold currents,[1,2] high wall-plug efficiencies,[3] low operating voltages,[4] and high fabrication yields.[5]

To quantify the effect of transverse-optical confinement and to facilitate further improvement of VCSEL properties it is necessary to have at our disposal an accurate optical model with which to study these effects. In this paper we use the model that we recently introduced in Ref. 6 for a more detailed investigation of the influence of transverse-optical confinement on threshold material gain and modal stability. We treat a variety of structures, including airpost and regrown VCSEL cavities and oxide-apertured structures with thin oxide layers.

The rest of the paper is structured as follows: For the sake of clarity, the main points of the model from Ref. 6 are briefly outlined in Section 2. In Section 3 we compare the performance of airpost and regrown VCSEL's at 1.55 μm, and in Section 4 we concentrate on oxide-apertured devices at 980 nm.

2. DESCRIPTION OF THE MODEL

Previously developed VCSEL models were based mostly on either scalar equations[7-9] or approximate vectorial equations.[10,11] However, for structures with dimensions of the order of the wavelength and with strong index contrasts (e.g., oxide-apertured devices), a rigorous vectorial approach seems to be more appropriate, especially for the study of polarization properties of higher-order transverse modes.

There has already been some effort to develop vectorial optical models for VCSEL structures. In Refs. 12 and 13 exact but computationally intensive vectorial models were presented. References 14 and 15 both outline similar methods based on eigenmode expansion but are unable to model diffraction because only guided modes are included in the expansion.

The model that we presented in Ref. 6 is also based on vectorial eigenmode expansion, but, because both the guided and the radiation modes are included, diffraction effects can be modeled as well. Moreover, inasmuch as the gain profile in the active region can be taken into account explicitly, hot-cavity calculations are possible.

To discretize the radiative mode spectrum of the cavity, we enclose the structure under study within a perfectly conducting metal cylinder (Fig. 1). Provided that the radius of this cylinder is sufficiently large, the influence of parasitic reflections can be made negligible.

In each longitudinally invariant layer i of the structure, we express the total field as a superposition of the forward ($+$) and backward ($-$) propagating eigenmodes of that particular layer:

$$\mathbf{E}_i^{\text{tot}}(r, \varphi, z) = \sum_k \{A_{i,k}{}^+ \mathbf{E}_{i,k}(r, \varphi)\exp(-j\beta_{i,k} z) \\ + A_{i,k}{}^- \mathbf{E}_{i,k}(r, \varphi)\exp(j\beta_{i,k} z)\},$$

$$\mathbf{H}_i^{\text{tot}}(r, \varphi, z) = \sum_k \{A_{i,k}{}^+ \mathbf{H}_{i,k}(r, \varphi)\exp(-j\beta_{i,k} z) \\ - A_{i,k}{}^- \mathbf{H}_{i,k}(r, \varphi)\exp(j\beta_{i,k} z)\}. \quad (1)$$
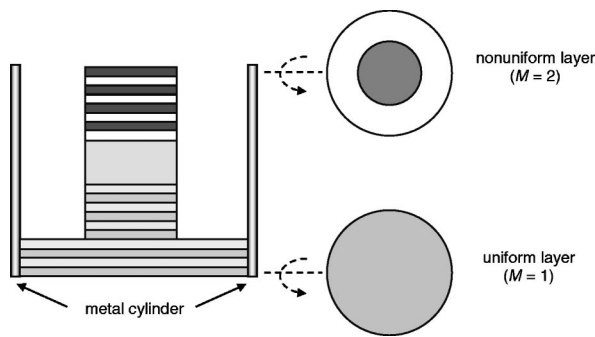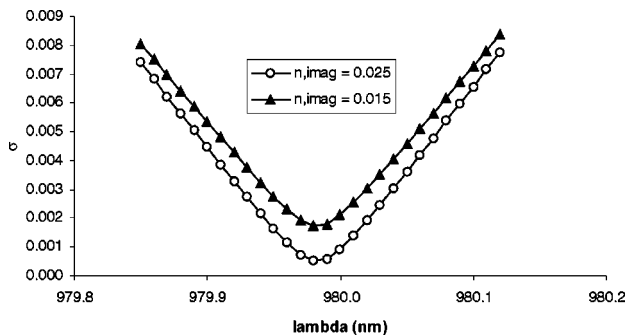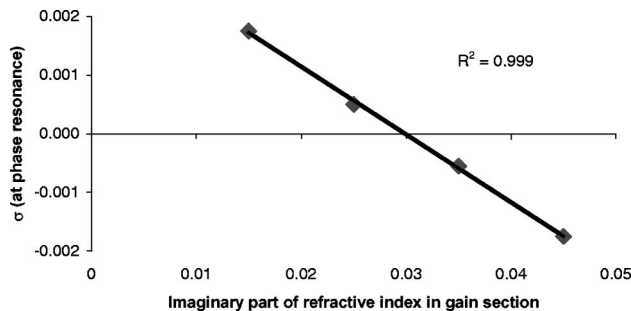
Fig. 1.   VCSEL model geometry.

Fig. 2.   Typical observed (λ, σ_i) plot.

Fig. 3.   Typical observed (gain, σ_i) plot at phase resonance.

When the cylinder is not homogeneously filled (i.e., $M > 1$), each of these eigenmodes is in turn written as a linear combination of the simpler eigenmodes of the uniformly filled cylinder ($M = 1$).   Thus we avoid having to solve the dispersion relation for $M > 1$ in the complex plane.

We calculate the reflection and transmission matrices at an interface between two layers by applying the so-called mode-matching technique.[16]   To determine the reflection and transmission matrices of an entire stack of layers, we use the well-known scattering matrix approach of Ref. 17.

The final step in the model consists of finding the laser mode of the cavity together with its threshold material gain.   To this end, we cut the cavity in half at an arbitrary z position, e.g., in the middle of the active layer. With the procedure outlined in the previous paragraphs, we calculate the reflection matrix $\mathbf{R}_{\text{top}}$ that describes the reflection of the top part of the cavity for fields incident from the bottom part.   Similarly, we can derive the reflection $\mathbf{R}_{\text{bot}}$ of the bottom part as seen from the top.   The vector $\mathbf{a}$, which contains the expansion coefficients of a la-

ser mode, must satisfy the resonance condition that expresses a round-trip gain of unity:

$$\mathbf{R}_{\text{top}}\mathbf{R}_{\text{bot}}\mathbf{a} = \mathbf{a}. \tag{2}$$

This is equivalent to looking for eigenvalues of the matrix $\mathbf{R} = \mathbf{R}_{\text{top}}\mathbf{R}_{\text{bot}}$ that have an eigenvalue of 1.   To enhance the numerical stability it is more appropriate to perform a singular-value decomposition of $\mathbf{R} - \mathbf{1}$, where $\mathbf{1}$ is the unit matrix.   It can be proved that, if a singular value of this matrix is zero, an eigenvector with an eigenvalue 1 of matrix $\mathbf{R}$ has been found.

To locate a laser mode we proceed as follows: For a given value of the material gain g_{mat}, we calculate the singular value σ_i at different wavelengths.   Typically, σ_i describes a hyperbola as a function of the wavelength (Fig. 2).   The minimum of this hyperbola corresponds to phase resonance.   After we have located the lasing wavelength in this way, we keep λ fixed and calculate σ_i for different gain levels g_{mat} in the active region (Fig. 3).   In this way we can determine the threshold material gain for this particular laser mode.

3.   AIRPOST AND REGROWN VERTICAL-CAVITY SURFACE-EMITTING LASERS

Recently, VCSEL's operating at 1.55 μm were realized, based on an InP bottom mirror and a dielectric Si/SiO$_2$ mirror.[18,19]   In Ref. 19 it was argued that one could decrease diffraction losses in these devices by etching the bottom mirror (Fig. 4) or by regrowing the airpost by semi-insulating InP (Fig. 5).   Here we evaluate these effects, using the model just presented.

Figures 6 and 7 show the threshold material gain for a uniform gain profile in an active region of 5-nm thickness. Parameters that are varied in the simulations are device diameter (5 or 10 μm) and etch depth (10, 20, or 30 mirror pairs from a total of 50).   As expected, smaller devices suffer from increased diffraction loss, leading to a higher threshold gain.   For the airpost structure without regrowth, Fig. 6 shows that increasing the etch depth leads
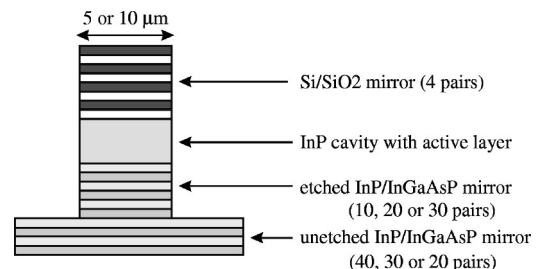

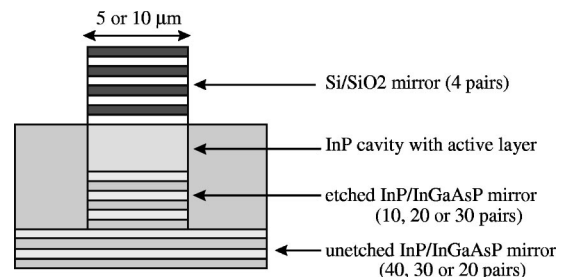Fig. 4.   Airpost VCSEL structure.

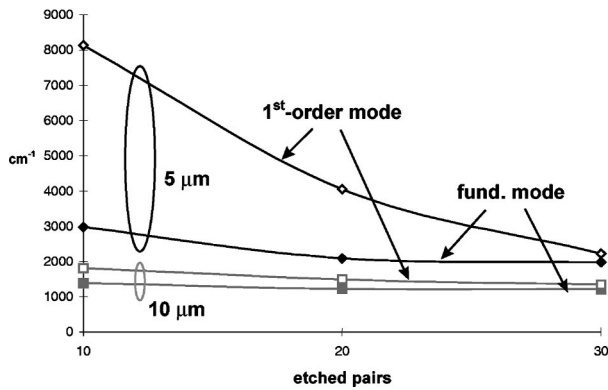Fig. 5.   Regrown VCSEL structure.

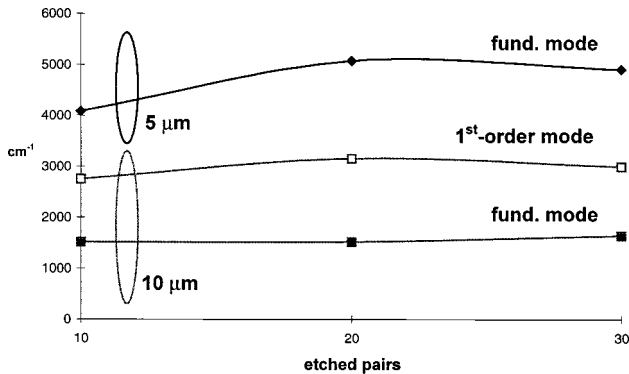Fig. 6. Threshold material gain (airpost VCSEL).

Fig. 7. Threshold material gain (regrown VCSEL).

to a lower threshold. The longer waveguide that is created by deeper etching helps to confine the mode to the core of the structure, thereby reducing diffraction losses. In the regrown structure (Fig. 7) we see a different behavior. The lower index contrast given by the regrown InP does not provide for enough guiding, so a significant fraction of the field will spread out to the cladding layers. The reflectivity seen by this cladding field decreases as the etch depth is increased, because of the ever-lower number of mirror pairs left in the cladding. This decrease leads to an increase in threshold gain for increasing etch depth. Only for deep etches does the threshold gain decrease again, indicating that the less pronounced waveguiding has ultimately become strong enough to counteract the lower cladding reflectivity. Finally, we note that the threshold for regrown devices is always larger than for airpost structures.

We can assess modal stability by comparing the threshold gain of the fundamental mode and of the higher-order transverse modes. Looking again at Fig. 6, we can see that this threshold difference is larger for smaller devices, as the larger diffraction losses in small components have a greater effect on the badly guided higher-order mode. For deep etches, the threshold of the higher-order mode approaches that of the fundamental mode. This indicates that both modes are almost perfectly confined within the waveguide core, so diffraction losses for both modes are negligible. From Fig. 7 it is also apparent that the gain difference is much larger in the regrown case than in the airpost case, because of the lower index contrast. This is especially true for the small devices, for

which we were unable to accurately pinpoint the higher-order mode, because it was already close to cutoff.

Finally, it can be seen that, for small devices, there is always a trade-off between low threshold for the fundamental mode and a good modal stability: The etch depth with the lowest threshold for the fundamental mode yields the poorest modal stability.

The trends from Figs. 6 and 7 agree well with experimental optical pumping results of Ref. 20, which show, e.g., that regrown structures generally have a slightly higher threshold than airpost structures. However, regrown devices lased down to smaller diameters compared with airposts, although the model predicts the opposite. This result can be explained by the fact that the regrown InP is a good heat conductor, allowing for more-efficient cooling of the regrown devices.

It is also interesting to compare the results obtained here with those presented in Ref. 21. There, an airpost structure was analyzed for which the etching occurred only in the top distributed Bragg reflector (DBR). Another noted difference is the use of an AlGaAs top DBR instead of a Si/SiO_2 top DBR. In spite of these differences, these simulations also predict lower losses for increasing etch depths. A feature of Ref. 21 that is not clearly reproduced in our results is the oscillations in the losses as a function of the etch depth. However, it should be noted that the structure that we consider here is much more deeply etched than the one treated in Ref. 21 and that, furthermore, in the device described in Ref. 21 the amplitude of these oscillations decreases when the etch depth increases.

4. OXIDE-APERTURED VERTICAL-CAVITY SURFACE-EMITTING LASERS

In this section we evaluate the benchmark modeling task from Ref. 22, for which a thin ($\lambda/20$) oxide is placed at five different positions within a $\lambda/4$ DBR layer. The laser structure under study is a 980-nm emitting device with a 30-period bottom DBR and a 25-period top DBR (Fig. 8). The gain in the active region is assumed to be constant and confined within the oxide diameter, which is 4 μm in this example.

Figure 9 compares the threshold material gain for both the fundamental and the first-order modes for the different aperture positions. For reference, these values are also given in the absence of any oxide and in the case of a thick $\lambda/4$ oxide.

It is clear that an antinode oxide leads to a much reduced threshold gain, as was also found in Ref. 13. Indeed, the aperture is placed at a maximum of the standing-wave pattern and is therefore very effective in
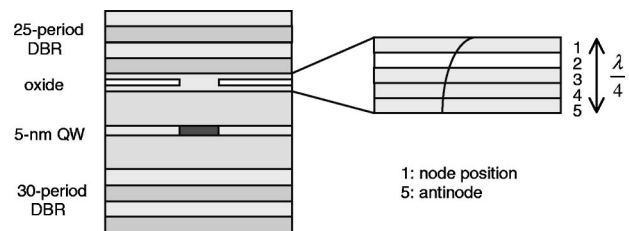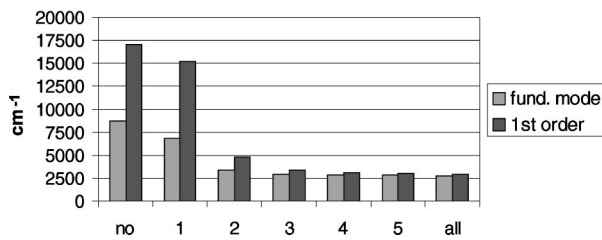

Fig. 8. Al-oxidized VCSEL.

Bienstman *et al.*

Fig. 9.   Threshold material gain (oxidized VCSEL):   1, node oxide; 5, antinode oxide; no, no oxide; all, λ/4 oxide.

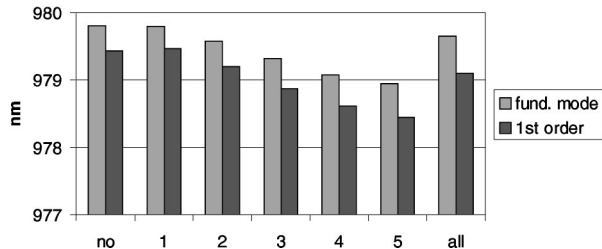

Fig. 10.   Lasing wavelength (oxidized VCSEL):   1, node oxide; 5, antinode oxide; no, no oxide; all, λ/4 oxide.

counteracting diffraction.   However, this is true for both the fundamental mode and the higher-order modes. Therefore an antinode oxide is able to provide for low-threshold gain for the fundamental mode but does so at the expense of a reduced modal selectivity.

In a node oxide exactly the opposite is true.   The aperture is placed at a field minimum and is not very effective in counteracting diffraction.   These detrimental diffraction effects are worse for the higher-order modes, and therefore a node oxide provides for good modal stability but does so at the expense of a higher threshold for the fundamental mode.

In Fig. 10 the resonance wavelength of these structures is plotted for both the fundamental mode and the higher-order mode.   All the structures exhibit a clear blueshift with respect to the design wavelength of 980 nm.   Antinode oxides give rise to larger shifts because of the increased interaction with the aperture at the field maximum.   Similar blueshifts were also observed in the research reported in Ref. 12.   It is also interesting that the thick $\lambda/4$ oxide leads to thresholds that are approximately as low as for the thin antinode oxide but does so at smaller blueshifts.

5.   CONCLUSION

We have presented a vectorial electromagnetic model that is capable of determining the optical properties of currently used VCSEL's.   For different structures, we demonstrated the trade-off that needs to be made between low threshold for the fundamental mode and good modal stability.

ACKNOWLEDGMENTS

P. Bienstman's e-mail address is peter.bienstman @rug.ac.be.

*Present address, Barco R&D Department, Th. Sevenslaan 106, B-8500 Kortrijk, Belgium.

REFERENCES

1.   E. R. Hegblom, N. M. Margalit, A. Fiore, and L. A. Coldren, "Small efficient vertical cavity lasers with tapered oxide apertures," Electron. Lett. **34**, 895–897 (1998).
2.   D. L. Huffaker and D. G. Deppe, "Improved performance of oxide-confined vertical-cavity surface-emitting lasers using a tunnel injection active region," Appl. Phys. Lett. **71**, 1449–1451 (1997).
3.   K. L. Lear, K. D. Choquette, R. P. Schneider, S. P. Kilcoyne, and K. M. Geib, "Selectively oxidized vertical cavity surface emitting lasers with 50% power conversion efficiency," Electron. Lett. **31**, 208–209 (1995).
4.   K. D. Choquette, R. P. Schneider, K. L. Lear, and K. M. Geib, "Low threshold voltage vertical cavity lasers fabricated by selective oxidation," Electron. Lett. **30**, 2043–2044 (1994).
5.   K. D. Choquette, K. L. Lear, R. P. Schneider, K. M. Geib, J. J. Figiel, and R. Hull, "Fabrication and performance of selectively oxidized vertical cavity lasers," IEEE Photon. Technol. Lett. **7**, 1237–1239 (1995).
6.   B. Demeulenaere, P. Bienstman, B. Dhoedt, and R. Baets, "Detailed study of AlAs-oxidized apertures in VCSEL cavities for optimized modal performance," IEEE J. Quantum Electron. **35**, 358–367 (1999).
7.   G. R. Hadley, "Effective index model for vertical-cavity surface-emitting lasers," Opt. Lett. **20**, 1483–1485 (1995).
8.   G. R. Hadley, K. L. Lear, M. E. Warren, K. D. Choquette, J. W. Scott, and S. W. Corzine, "Comprehensive numerical modeling of vertical-cavity surface-emitting lasers," IEEE J. Quantum Electron. **32**, 607–616 (1996).
9.   G. R. Hadley, "Low-truncation-error finite difference equations for photonics simulation.   II. Vertical-cavity surface-emitting lasers," J. Lightwave Technol. **16**, 142–151 (1998).
10.   M. J. Noble, J. P. Loehr, and J. A. Lott, "Analysis of microcavity lasing modes using a full-vector weighted index method," IEEE J. Quantum Electron. **34**, 1892–1903 (1998).
11.   M. J. Noble, J. P. Loehr, and J. A. Lott, "Semi-analytic calculation of diffraction losses and threshold currents in microcavity VCSELs," in *IEEE LEOS Annual Meeting* (Institute of Electrical and Electronics Engineers, Piscataway, N.J., 1998), pp. 212–213, paper WI3.
12.   M. J. Noble, J. P. Loehr, and J. A. Lott, "Quasi-exact optical analysis of oxide apertured microcavity VCSEL's using vector finite elements," IEEE J. Quantum Electron. **34**, 2327–2339 (1998).
13.   B. Klein, L. F. Register, K. Hess, D. G. Deppe, and Q. Deng, "Self-consistent Green's function approach to the analysis of dielectrically apertured vertical-cavity surface-emitting lasers," Appl. Phys. Lett. **73**, 3324–3326 (1998).
14.   D. Burak and R. Binder, "Cold-cavity vectorial eigenmodes of VCSEL's," IEEE J. Quantum Electron. **33**, 1205–1215 (1997).
15.   R. Kuszelewicz and G. Aubert, "Modal matrix theory for light propagation in laterally restricted stratified media," J. Opt. Soc. Am. A **14**, 3262–3272 (1997).
16.   W. C. Chew, *Waves and Fields in Inhomogeneous Media* (Van Nostrand Reinhold, New York, 1990).

17. L. Li, "Formulation and comparison of two recursive matrix algorithms for modeling layered diffraction gratings," J. Opt. Soc. Am. A **13**, 1024–1035 (1996).
18. S. Rapp, J. Piprek, K. Streubel, J. André, and J. Wallin, "Temperature sensitivity of 1.54 μm vertical cavity lasers with an InP-based Bragg reflector," IEEE J. Quantum Electron. **33**, 1839–1845 (1997).
19. K. Streubel, S. Rapp, J. André, and J. Wallin, "Room-temperature pulsed operation of 1.5 μm vertical cavity lasers with an InP-based Bragg reflector," IEEE Photon. Technol. Lett. **8**, 1121–1123 (1996).

20. T. Heide, "Steady state and modal properties of vertical cavity surface emitting lasers," M.S. thesis (Royal Institute of Technology, Stockholm, 1996).
21. G. Liu, J.-F. Seurin, S. L. Chuang, D. I. Babic, S. W. Corzine, M. Tan, D. C. Barnes, and T. N. Tiouririne, "Mode selectivity study of vertical-cavity surface-emitting lasers," Appl. Phys. Lett. **73**, 726–729 (1998).
22. COST 268 modeling exercise (http://www.ele.kth.se/COST268/WG1/WGExcercise1.html), based on R. Kuszelewicz, Centre National d'Etudes en Télécommunication, Paris (personal communication, 1998).